Vol. 31, No. 3 Journal of Semiconductors March 2010

Fluid model of inductively coupled plasma etcher based on COMSOL*

Cheng Jia(程嘉)[1,†], Ji Linhong(季林红)[1], Zhu Yu(朱煜)[1], and Shi Yixiang(史翊翔)[2]

(1 State Key Laboratory of Tribology, Tsinghua University, Beijing 100084, China)
(2 Department of Thermal Engineering, Tsinghua University, Beijing 100084, China)

Abstract: Fluid dynamic models are generally appropriate for the investigation of inductively coupled plasmas. A commercial ICP etcher filled with argon plasma is simulated in this study. The simulation is based on a multiphysical software, COMSOL™, which is a partial differential equation solver. Just as with other plasma fluid models, there are drift–diffusion approximations for ions, the quasi-neutrality assumption for electrons movements, reduced Maxwell equations for electromagnetic fields, electron energy equations for electron temperatures and the Navier–Stokes equation for neutral background gas. The two-dimensional distribution of plasma parameters are shown at 200 W of power and 1.33 Pa (10 mTorr) of pressure. Then the profile comparison of the electron number density and temperature with respect to power is illustrated. Finally we believe that there might be some disagreement between the predicted values and the real ones, and the reasons for this difference would be the Maxwellian eedf assumption and the lack of the cross sections of collisions and the reaction rates.

Key words: inductively coupled plasma; simulation; COMSOL
DOI: 10.1088/1674-4926/31/3/032004 **PACC:** 5265

1. Introduction

Inductively coupled plasmas (ICP) sources are widely used in etching and deposition, etc, because of high density and low operation pressure. During recent decades there has been a growing interest in modeling and simulation for the ICP sources[1]. At present, the plasma modeling is used as a significant assistant in the development of new equipments and the improvement of process control schemes in semiconductor equipment manufacturers. An accurate plasma discharge model is hardly achieved, for the lack of the essential information in plasma, such as the collision cross sections, the chemical reaction rates and the surface coefficients. Although there are usually some differences between the plasma models and the experimental results, much effort has been made in using simulation to explain some phenomena and enhance the process. Meanwhile there are numerical simulation techniques for plasma discharge, where the most important methods include fluid dynamic, kinetic and hybrid models. Three simulation models are significantly different in principles, strengths and limitations. So there is no so-called "the best" model as the criteria for a certain selected plasma tool, if appropriate assumptions are made[2]. The kinetic models, such as PIC-MCC, are used for more precision, and the fluid models are for quick computation and barely basic accuracy, and then the hybrid models are in balance of precision and efficiency. In spite of this, the fluid model is also able to keep the computational accuracy even at very low pressure[3]. In this paper the fluid model is appropriate and sufficient for the plasma experiment.

It is well-known that gaseous electronics conference RF reference cell (GECRC) was conceived to serve as a convenient test system for experimental and modeling studies. In another paper (not published), we had simulated the GECRC in ICP mode with the fluid model, and then compared with the measured values obtained from this system. This research provides evidence to confirm the validity of our plasma fluid model based on COMSOL™.

COMSOL is a PDE (partial differential equation) solver which comes from MATLAB™[4]. Users could conveniently formulate physical equations in three ways according to their requirements, and don't have to spend more time in coding and numerical algorithm. In this paper, firstly the fluid plasma model and numerical method are described detailedly. Then the argon discharge in a commercial ICP etcher system is compared with the simulation based on COMSOL™. Finally the prediction results and the analysis are both discussed.

2. Description of the plasma fluid model

Concerning the plasma fluid models there are lots of previous publications discussed, and in this paper our model is mainly based on them[5−10]. Each species is considered as a separated fluid to satisfy mass conservation in all computational regions. A Maxwellian distribution is assumed for electrons. In some conditions, this is a reasonable assumption while the electron energy is lower than 15 eV at low pressures[11]. The existence of a high energy tail of the electron energy distribution function (eedf) will be the main cause of disagreement in the electron energy. However the disagreement is acceptable in this paper, compared to other assumptions.

2.1. Mass conservation equations

For ions, electrons, and neutrals, three different transportation equations are provided to describe, which all follow mass conservation equations. The details are as follows.

* Project supported by the China Postdoctoral Science Foundation (No. 20080440376).
† Corresponding author. Email: chengjia@mails.thu.edu.cn
Received 20 September 2009, revised manuscript received 20 October 2009 © 2010 Chinese Institute of Electronics

Table 1. Important collision parameters in the argon discharge.

Reaction		$k_r(T_e) = \alpha_{1r}\exp(-2r/T_e)$		ε_r (eV)‡
		α_{1r} (10^{-13} m^3/s) †	α_{2r} (eV) †	
Ionization	$e + Ar \rightarrow Ar^+ + e + e$	1.2	18.7	15.6
Excitation	$e + Ar \rightarrow Ar^* + e$	0.12	11.94	11.6
Step-wise ionization	$e + Ar^* \rightarrow Ar^+ + e + e$	3	5.22	4.14

†Comes from CFD-ACE+ 2004, which refers to JILA collision cross-section database in Colorado University. ‡Comes from Ref. [6].

2.1.1. For ions

Ions continuity assumption is valid, and electric field force drives efficiently ions, so ions conservation equation is

$$\frac{\partial n_i}{\partial t} = 0 = S_i - \nabla \cdot J_i. \quad (1)$$

where n_i and J_i are the ion number density and the ion flux, respectively. Considering this model as steady static, we let $\partial n_i/\partial t = 0$. The source or sink of ions, S_i, is determined by the product of reaction ion number density and reaction rate coefficient as follows,

$$S_i = \sum_{j,k} K_{jk}(T_e)\, n_j n_k, \quad (2)$$

where $K_{jk}(T_e)$ is the reaction rate coefficient which is generally related with the electron temperature, T_e, just as Table 1 has shown; n_j and n_k are number densities of the two species which collide (react) each other to generate ions in plasma (two species collision is common in low temperature plasma.). The important collision parameters of argon plasma are listed in Table 1.

In Table 1, the symbols +, *, and e denote positive ions, metastable atoms and electrons, respectively. ε_r indicates the reaction energy in the corresponding equation.

In this paper, the drift–diffusion approximation is used to describe the ions fluxes. This appears to be a good approximation for $K_n < 0.2$ ($\sim$10 mTorr for typical ICPs)[6].

$$J_i = -D_i \nabla n_i + z_i \mu_i n_i E_S, \quad (3)$$

where z_i is the number of elementary charges on the ion. D_i and μ_i are the diffusivity and mobility of the ion.

$$D_i = \frac{kT_i}{m_i \nu_{in}}, \quad (4)$$

$$\mu_i = \frac{e}{m_i \nu_{in}}, \quad (5)$$

where k is the Boltzmann constant, T_i and m_i are the temperature and mass of the ion. The collision frequency between ions and neutral background species, ν_{in}, is given by

$$\nu_{in} = \sigma_{in} \bar{v}_i N, \quad (6)$$

where σ_{in} is the collision cross section, and $\bar{v}_i = \sqrt{8kT_i/\pi m_i}$ is the mean thermal movement velocity, and N is the number of neutral background species density. One of the main forces driving ions, the static electric field E_S, is induced by ambipolar diffusion (in next section for details).

In general, the sheath calculation in ICP models is treated as the boundary conditions of bulk plasma because of the non-collision in it. In this paper, the boundary condition of positive ions at the walls is represented by the Bohm flux, while the flux of negative ions is zero in the model,

$$J_{ibc} = n_i u B_i \hat{n} = n_i \sqrt{\frac{kT_e}{m_i}}\hat{n}, \quad (7)$$

where u_{Bi} is the Bohm velocity of positive ions, and $\hat{n}$ represents the normal vector towards the wall[6].

2.1.2. Quasi-neutrality for electrons

For ICP, many models consider that the quasi-neutrality constraint in the bulk plasma is applicable[6, 12]:

$$n_e = \sum_i z_i n_i. \quad (8)$$

where n_e is the electron number density, which is equal to the summation of all ions number densities everywhere.

In general, the static electric field mentioned above is solved from the Poisson equation especially in the sheath zone, but it is not necessary if the quasi-neutrality assumption is used to simplify the model. In this model no negative ion is considered, so for electrons in the thermal equilibrium state the static electric field can be obtained from the Boltzmann relation of electrons[6],

$$E_S = -\frac{k}{q n_e} \nabla (n_e T_e), \quad (9)$$

where q is the elementary charge.

2.1.3. For neutrals

Neutrals (refer to metastable atom, Ar*, in this model) are of no electric charge, so they are completely unaffected by the electromagnetic force. In argon plasma the ambipolar-diffusion is the main driving force for neutrals at low pressure. In active gas plasma (e.g., O_2, Cl_2), the contribution of gas flow is generally more important rather than diffusion, because the radical density depends on flow velocity[10]. For the reason of pressure grads at the chamber inlet, the convection term of the mass conservation equation for neutral species cannot be neglected,

$$\frac{\partial n_n}{\partial t} = 0 = S_n - \nabla \cdot (-D_n \nabla n_n + u_n n_n), \quad (10)$$

where D_n, u_n, and n_n are the diffusivity, convection velocity, and number density of the neutral species (metastable atom, Ar*). In Eq. (10), S_n indicates all source/sink reactions related to neutral species[6].

2.2. Electron energy equations

There are several theories on electron energy equations under different conditions[13−15]. In this paper, the electron energy balance is described by

$$\frac{\partial}{\partial t}\left(\frac{3}{2}n_{\mathrm{e}}kT_{\mathrm{e}}\right)+\nabla\cdot q_{\mathrm{e}}+eJ_{\mathrm{e}}\cdot E-P_{\mathrm{ind}}$$
$$+3\frac{m_{\mathrm{e}}}{M}n_{\mathrm{e}}k\nu_{\mathrm{m}}\left(T_{\mathrm{e}}-T_{\mathrm{g}}\right)+n_{\mathrm{e}}N\sum_{j}K_{j}\left(T_{\mathrm{e}}\right)\varepsilon_{j}=0, \quad (11)$$

where the second term is the divergence of the total electron energy flux, the third term stands for Joule heating, and P_{ind} represents the inductive heating, that is the power deposited into the plasma which is solved from electromagnetic field model. The fifth and sixth terms are energy loss in elastic/inelastic collisions between electrons and neutral species respectively. E is the static-electric field E_{S} induced by ambipolar-diffusion, which can be obtained from Eq. (9). T_{g} is the gas temperature (for convenience, in this case Ar, Ar^{+} and Ar^{*} are of the same temperature). The total electron energy flux is given by

$$q_{\mathrm{e}}=\frac{5}{2}kT_{\mathrm{e}}J_{\mathrm{e}}-K_{\mathrm{e}}\nabla T_{\mathrm{e}}, \quad (12)$$

where the thermal conductivity of electrons is $K_{\mathrm{e}}=3kD_{\mathrm{e}}n_{\mathrm{e}}/2$. In bulk plasma electron flux is equal to the summation of the ions flux through the ambipolar approximation:

$$J_{\mathrm{e}}=\sum_{\mathrm{i}\neq\mathrm{e}}J_{\mathrm{i}}. \quad (13)$$

The boundary conditions of the electron energy towards the wall was taken as

$$q_{\text{e-bc}}=\frac{5}{2}kT_{\mathrm{e}}J_{\text{e-bc}}\cdot\hat{n}=\frac{5}{2}kT_{\mathrm{e}}\sum_{\mathrm{i}\neq\mathrm{e}}J_{\text{i-bc}}\cdot\hat{n}, \quad (14)$$

where $\hat{n}$ represents the unit normal vector. The boundary conditions at the inlet/outlet of the chamber are set as Neumann conditions, $\hat{n}\cdot q_{\mathrm{e}}=0$.

2.3. Electromagnetic equations

Maxwell equations could be used in solving electromagnetic field, in the case of two-dimensional axisymmetric ICP model, these equations can be reduced in the form of magnetic vector A as

$$\frac{1}{\mu_{0}\mu_{\mathrm{r}}}\nabla^{2}A+\varepsilon_{0}\varepsilon_{\mathrm{r}}\omega^{2}A=-J_{\mathrm{S}}, \quad (15)$$

where $\boldsymbol{J}_{\mathrm{S}}$ is the current density in coils. Since high frequency (13.56 MHz) results in the skin effect, the current in coils is conducted by the coil surface. Once the distribution of electromagnetic field is obtained, the time-averaged value of the power density deposited in the plasma could be evaluated by

$$P_{\mathrm{ind}}=\frac{1}{2}\mathrm{Re}\left(\sigma_{\mathrm{p}}\right)\omega_{\mathrm{RF}}^{2}\left|A\right|^{2}, \quad (16)$$

where ω_{RF} is the angular frequency ($\omega_{\mathrm{RF}}=2\pi f_{\mathrm{RF}}$), and σ_{p} is the complex plasma conductivity,

$$\sigma_{\mathrm{p}}=\frac{n_{\mathrm{e}}e^{2}}{m_{\mathrm{e}}\left(\nu_{\mathrm{en}}+\mathrm{j}\omega_{\mathrm{RF}}\right)}, \quad (17)$$

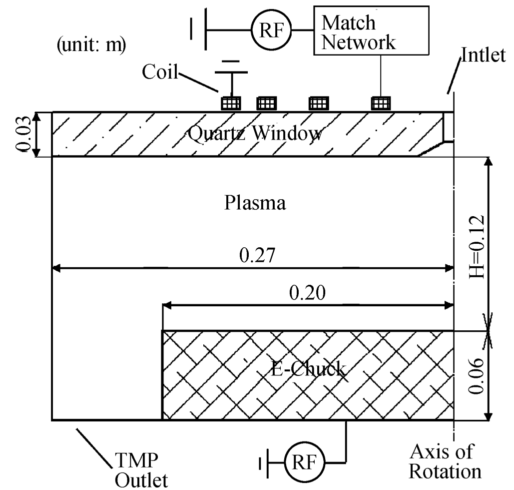

Fig. 1. Schematic diagram of the ICP etcher.

where m_{e} and ν_{en} represent the electron mass and effective momentum-transfer collision frequency respectively. The plasma dielectric constant ε_{p} is obtained from

$$\varepsilon_{\mathrm{p}}=\varepsilon_{0}\left(1-\mathrm{j}\frac{\sigma_{\mathrm{p}}}{\omega\varepsilon_{0}}\right), \quad (18)$$

where ε_{0} is the permittivity of vacuum.

2.4. Navier-Stokes equation for neutral background gas

Neutral background gas has an important influence on the distribution of plasma in two aspects: one is that the source/sink where plasma generates or dissipates is proportional to the number density of neutral gas; the other is that the number density of neutral gas can change the collision frequency of electrons and other particles. In consideration of the influence of neutral background gas and pressure distribution on plasma, argon background gas flow is described by incompressible Navier-Stokes equations in this model.

$$\rho\frac{\partial u}{\partial t}-\nabla\cdot\eta\left(\nabla u+(\nabla u)^{T}\right)+\rho u\cdot\nabla u+\nabla p=F, \quad (19)$$
$$\nabla\cdot u=0$$

where ρ, η, u represent gas density, dynamic viscosity and velocity vector respectively, P is pressure, and F is force. In this case the force is equal to zero. The boundary condition of inlet and outlet are set to velocity inlet type and pressure outlet respectively and the wall boundary condition is simply defined with the Dirichlet condition, that is $u=0$.

2.5. Set of COMSOL model

The two-dimensional axisymmetric schematic diagram of a commercial ICP etcher is given in Fig. 1. It shows that a flat spiral coil supplied by a 13.56 MHz radio frequency (RF) power above the quartz window generates plasma at low pressure. The process conditions of this system in this paper are at 1.33 Pa (10 mTorr), and from 100 to 500 W in RF power.

Users could use three application PDE modes (coefficient form, general form and weak form) to describe general equations. In this paper the mass conservation equations of ions and neutrals are described by the convection and diffusion

Table 2. Coefficients of the electron energy equation.

Coefficient	Expression or value
δ_{ts}	0（static state）
ρ	1
C_p	$-2.5k(D_i - 2kT_e/e)$
K	$3kD_e n_e/2 + 5\mu_i k^2 n_e T_e/2e$
Q	$Q = P_{ind} - Q_{ec} - Q_{ic} - Q_{joule} - Q_{other} = \frac{1}{2}Re(\sigma_p)\omega_{RF}^2 \lvert A\rvert^2 - 3\frac{m_e}{M}n_e k\nu_m (T_e - T_g)$ $-n_e N(K_{iz}\varepsilon_{iz} + K_{ex}\varepsilon_{ex}) - e(-D_i\nabla n_i + \mu_i E_S)E_S - \frac{5}{2}k\left(-D_i T_e - \frac{\mu_i k}{e}T_e^2\right)\nabla^2 n_e$
u	∇n_i

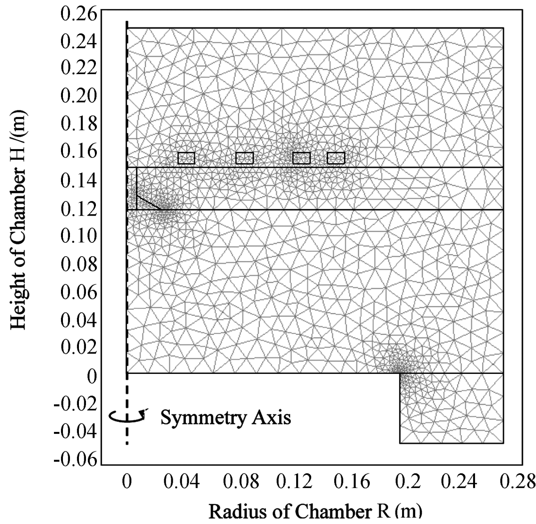

Fig. 2. Geometry and grids of ICP etcher.

equations in chemical engineering module (chcd). The electromagnetic field equation can be represented in the form of the perpendicular induction current equation (vector potential) in quasi-statics magnetic module (emqa). Also, the electron temperature balance equation is too hard to solve so that all energy source/sink is substituted by the source/sink term of the convection and condition in the heat transfer module (cc). According to the description of etcher mentioned above, the two-dimensional axisymmetric geometry with meshes of ICP etcher is shown in Fig. 2.

This COMSOL model is fulfilled with 2549 triangle meshes, although it wouldn't be enough if the Poisson equation was solved. When we refine meshes, the accuracy of result is not promoted obviously, which is to say that the meshes are enough in this model.

The coefficient form of the PDE is used to describe the electron energy equation which is one of the most complicated equations hardly solved in plasma fluid model. In COMSOL the heat transfer convection and condition equation is shown as follows, which is similar to the electron energy equation formally,

$$\delta_{ts}\rho C_p \frac{\partial T}{\partial t} + \nabla\cdot(-K\nabla T) + \rho C_p u \cdot \nabla T = Q. \quad (20)$$

We can compare Eq. (20) with the form of Eq. (11), and then conclude the corresponding coefficients of PDE, as listed in Table 2. The total energy source/sink Q includes P_{ind} (inductive heating), Q_{ec} (elastic collision heating), Q_{ic} (inelastic collision heating) and Q_{joule} (Joule heating) and the power term separated from the divergence of the energy flux.

For the electron temperature T_e, the energy balance equation is too high non-linear to solve. Also, there are the strong coupled variables T_e and n_e in the mass and energy balance equations, so the two equations must be directly solved altogether and the magnetic vector A is the middle variable to connect the energy balance and the electromagnetic equation through the inductive power P_{ind}.

3. Results and discussions

In general experiments the measurement data is often one-dimension, however in simulation plasma parameters distribution profiles can be of two-dimensions. Figure 3 shows the results of electron temperature and electron density distribution in the chamber at 1.33 Pa (10 mTorr) and 200 W. The electron temperature is the highest under the window just between the 2nd and the 4th coil turn, where the dissipated power density is also the highest (shown in Fig. 4(b)). Under the diffusion and recombination of ions and electrons at the wall, the electron density is higher in the central chamber than near walls. And then we can find that Figure 4 describes the profiles of azimuthal electric field and dissipated power density in the same conditions as well. And also the max electric field intensity and power density is 1114.39 V/m and 2.415×10^5 W/m^3, respectively. From Fig. 4, it is proposed that there is certain numberical relation between power density and azimuthal electric field through the electric conductivity.

In Fig. 5 the metastable atom density and ionization rate are shown as follows. There is a difference in distribution shape between Fig. 3 (b) and Fig. 5 (a). That is to say that the electron density profile is almost symmetric between up-down walls, but the center of metastable atom density profile is closer to upper wall. The main reason for this situation is because of the main driving forces of them. In the drift–diffusion approximation, the electric-static field induced by ambipolar diffusion dominates the movement of ions, which is responded rapidly by electrons. However for the metastable atom the main driving force is diffusion and the density of background argon gas is higher near the inlet. According to the definition of the source term of the ions mass conversation, the ionization rate will increase with the electron density and temperature. So we can find that Figure 5(b) implies this relation.

The predicted electron density profiles changing with respect to power are shown in Fig. 6. The simulated data is in the radial direction 5 mm above the wafer. The electron density in

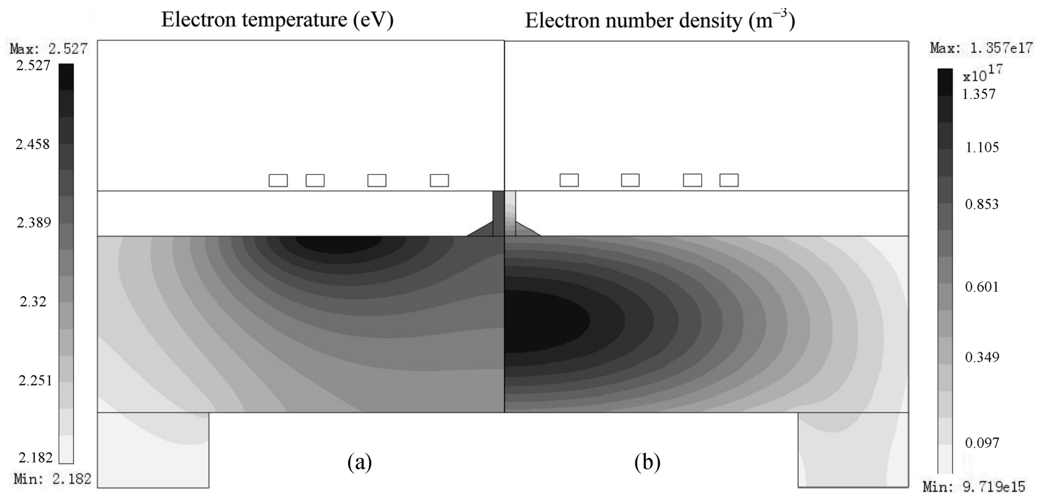

Fig. 3. (a) Electron temperature and (b) electron density distributions.

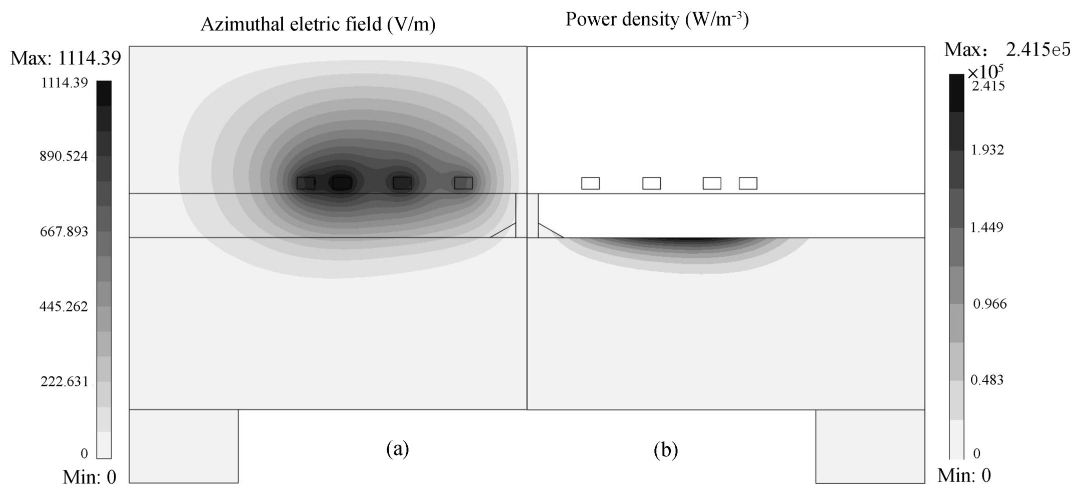

Fig. 4. (a) Azimuthal electric field and (b) power density distributions.

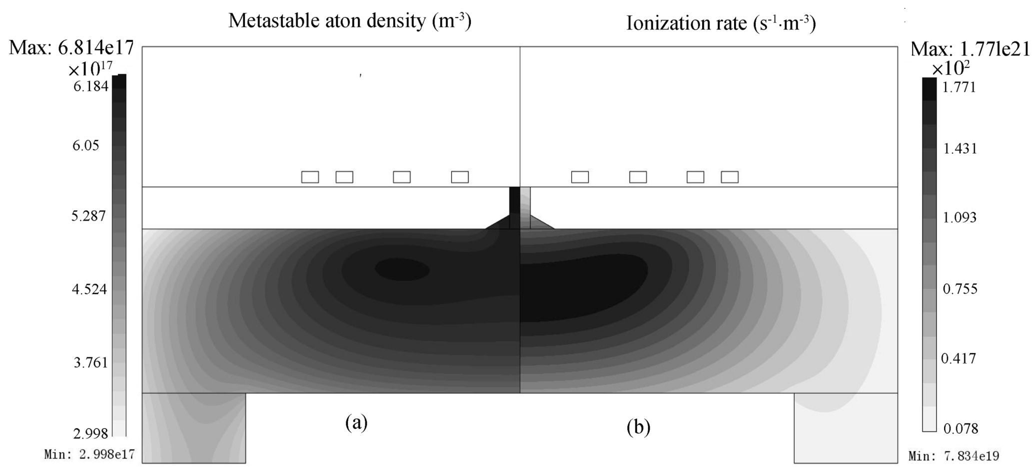

Fig. 5. (a) Metastable atom density and (b) ionization rate distributions.

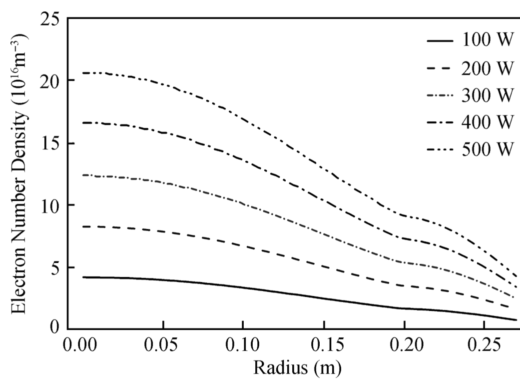

Fig. 6. Electron number density radial profiles for different RF powers 5 mm above electrostatic chuck.

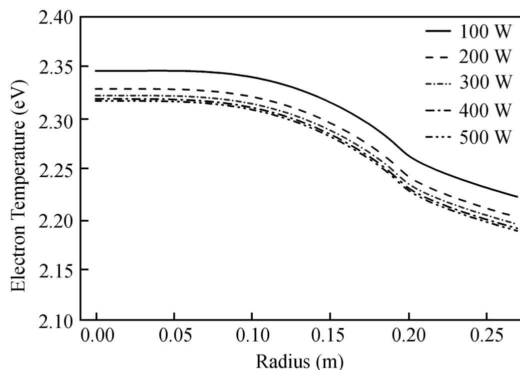

Fig. 7. Electron temperature radial profiles for different RF powers 5 mm above electrostatic chuck.

the central chamber at each power level is higher than the one near the sidewall. There is an inflexion for electron density at the edge of the electrostatic chuck. It is clear that the electron density increases with the dissipated power in proportion, because of ionization rate increasing as well.

From Fig. 7 we could conclude that there is no clear variation in the electron temperatures with power, just like Reference [16] shows. Although the experiment system built by Miller and his co-workers is smaller than the etcher in this study and there is some difference between them, researchers could hardly find out the relations of electron temperature and power. From the conclusion above, we can find that the electron number density and the total electron energy will both increase with the power. So the electron temperature hardly changes when the power increases. Besides this study, our previous research results in the same conclusion[17]. As we mentioned above, there might be the disagreement of predicted values and experimental measurement, which can be explained by using of the Maxwellian eedf in the model. In the real discharge, the high energy tail of Maxwellian is depleted for ionization. So when we assume the eedf is Maxwellian, the required mean electron energy is lower than the true values[11]. If we apply with an offline method to calculate the true eedf and reaction rate, we would make the prediction more accurate.

4. Conclusions

A commercial inductively coupled plasma etcher filled with argon is simulated on the COMSOL platform. We present that the electron number density increases with the dissipated power, and then the power has little effect on the electron temperature, as seen in other research[16,17]. In addition, we believe that there should be disagreement between the simulation and the real values, although the distribution profiles are of similar shape in the changing trend. The most important factor of disagreement is that the electron follows the Maxwellian distribution assumption. In addition, the lack of reasonably accurate cross sections makes the disagreement worse. An offline computational method which can calculate more quantitively accurate eedf and other plasma coefficients would be a perfect way, such as the Boltzmann equation solver. This is an area of our current research.

References

[1] Lymberopoulos D P, Economou D J. 2-dimensional self-consistent radio-frequency plasma simulations relevant to the gaseous electronics conference RF reference cell. J Res Natl Inst Stand Technol, 1995, 100(4): 473

[2] Kim H C, Iza F, Yang S S, et al. Particle and fluid simulation of low-temperature plasma discharges: benchmarks and kinetic effects. J Phys D: Appl Phys, 2005, 38: R283

[3] Surendra M. Radiofrequency discharge benchmark model comparison. Plasma Sources Sci Technol, 1995, 4: 56

[4] COMSOL 3.2, Userbook

[5] Lymberopoulos D P, Economou D J. Fluid simulations of glow discharges: effect of metastable atoms in argon. J Appl Phys, 1993, 73(8): 3668

[6] Panagopoulos T, Kim D, Vikas M, et al. Three-dimensional simulation of an inductively coupled plasma reactor. J Appl Phys, 2002, 91(5): 2687

[7] Brcka J. Modeling remote H_2 plasma in semiconductor processing tool. Proceedings of the COMSOL Users Conference, Boston, 2006

[8] Lymberopoulos D P, Economou D J. Two-dimensional simulation of polysilicon etching with chlorine in a high density plasma reactor. IEEE Trans Plasma Sci, 1995, 23(4): 573

[9] Novikova T, Kalache B, Bulkin P. Numerical modelling of capacitively coupled hydrogen plasma: effects of frequency and pressure. J Appl Phys, 2003, 93(6): 3198

[10] Lymberopoulos D P, Economou D J. Modeling and simulation of glow discharge plasma reactors. J Vac Sci Technol A, 1994, 12(4): 1229

[11] Bukowski J D, Graves D B, Vitello P. Two-dimensional fluid model of an inductively coupled plasma with comparison to experimental spatial profiles. J Appl Phys, 1996, 80(5): 2614

[12] CFD-ACE+ 2008, Userbook

[13] Jaeger E F, Berry L A, Tolliver J S, et al. Power deposition in high-density inductively coupled plasma tools for semiconductor processing. Phys Plasmas, 1995, 2(6): 2597

[14] Lee M H, Chung C W. On the E to H and H to E transition mechanisms in inductively coupled plasma. Phys Plasmas, 2006, 13: 063510

[15] Rauf S, Kushner M J. Model for noncollisional heating in inductively coupled plasma processing sources. J Appl Phys, 1997, 81(9): 5966

[16] Miller P A, Hebner G A, Greenberg K E, et al. An inductively-coupled plasma source for the gaseous electronics conference RF reference cell. J Res Natl Inst Stand Technol, 1995, 100(4): 427

[17] Cheng Jia, Zhu Yu, Wang Jinsong. Two-dimensional discharge simulation of inductively coupled plasma etcher. Chinese Journal of Semiconductors, 2007, 28(6): 989